Nonspecular x-ray reflection from rough multilayers

V. Holý
Department of Solid State Physics, Faculty of Science, Masaryk University, Kotlářská 2, 611 37 Brno, Czech Republic

T. Baumbach
Institut Laue-Langevin, Boîte Postale 156, Avenue des Martyrs, F-38042 Grenoble Cedex 9, France
(Received 18 October 1993)

X-ray reflection from periodical multilayers with randomly rough interfaces has been described within the distorted-wave Born approximation. The method is suitable for calculating both specular x-ray reflection and nonspecular (diffuse) scattering. In this paper, both in-plane and vertical correlations of the roughness profiles have been considered and it has been demonstrated that the vertical roughness correlation substantially affects the nonspecular scattering. The theory can explain resonant effects observed in the beam scattered nonspecularly from a periodical multilayer. The theoretical approach has been used for the study of interfacial roughness in a long-periodic AlAs/GaAs multilayer and good agreement has been achieved between the experimental results and the theory.

I. INTRODUCTION

X-ray reflection has frequently been used for structure studies of crystalline and amorphous layers and multilayers. By measuring the specular reflectivity, the thicknesses and electron densities of the layers can be determined and, also, root-mean-square (rms) roughnesses of the interfaces can be estimated. From the nonspecular reflectivity (diffuse scattering), the correlation function of the interface roughness profile can be reconstructed.

The specularly reflected (SXR) wave consists of the coherent wave and of the part of the incoherent wave propagating in the direction of specular reflection. The nonspecularly reflected wave (NSXR) is incoherent. If we neglect the divergence of the primary wave irradiating the sample, the coherent wave is plane and the incoherent wave is divergent (diffuse). The latter can be described using the mutual coherence function or the formalism of the differential scattering cross section.

Several theoretical descriptions of x-ray reflection from rough multilayers can be classified into two groups—kinematical and dynamical methods. In the kinematical approach the x-ray reflection is described within the concept of scattering processes from separate electrons, while extinction and multiple scattering are neglected.[1–7] This method [the first Born approximation (BA)] is suitable for coherent and incoherent scattering calculations and it can explain both SXR and NSXR. The BA is valid if the angles of the primary and emitted beams with the sample surface are large with respect to the critical angle θ_c of the total external reflection (TER). Near θ_c the BA method fails, since it neglects the x-ray refraction and TER.

Dynamical methods take account of multiple x-ray scattering and therefore include the effect of TER. In the coherent approximation the dynamical calculations lead to the well-known concept of the effective complex reflectivity of a rough interface.[8,9] This reflectivity equals that of a flat interface multiplied by an attenuation coefficient analogous to the static Debye-Waller factor. In the incoherent approach[7,10] the dynamical calculations can be performed on the basis of the distorted-wave Born approximation (DWBA). This method is applicable if the incidence and exit angles are not too large.

Specular reflectivity curves of periodical multilayers exhibit regularly distributed maxima analogous to diffraction satellites occurring by x-ray diffraction on monocrystalline periodical multilayers. Similar regular peaks have been observed previously in the nonspecularly scattered wave.[11,12]

In our previous paper[13] we have calculated the intensity of NSXR from thin layers and multilayers using the DWBA. We demonstrated that resonant maxima occur in the NSXR wave if the incidence and/or exit angles equal θ_c (so-called Yoneda wings). In the case of a layered system, additional resonant peaks occur if the angles of incidence or exit coincide with the angular position of a maximum of the coherent reflectivity.

The aim of this paper is to study the NSXR in periodical multilayers. Using the DWBA we calculate the distribution of the NSXR intensity in reciprocal space and show the influence of the correlation of roughness profiles of different interfaces on the NSXR distribution. The method is used for the study of interface roughness of a periodical AlAs/GaAs multilayer and a good agreement between theory and experiments is achieved.

II. THEORY

Let us consider a multilayer containing N interfaces ($N-1$ layers). Each layer is characterized by its refractive index n_j, local thickness $D_j(x,y)$ and mean thickness D_j^{id}. The jth interface lies between the jth and $(j+1)$th layers, and the interface $j=1$ is the free surface. The z

axis is perpendicular to the surface and its origin lies at the surface ($z_1 = 0$); the x axis lies in the incidence plane. The roughness profile of the j th interface is described by the random function $U_j(x,y)$ (Fig. 1).

In the Fraunhofer approximation the energy flux of the wave scattered into an elementary solid angle $d\Omega$ is proportional to the differential scattering cross section[7]

$$d\sigma = \langle |V_{12}|^2 \rangle / (16\pi^2) d\Omega, \tag{1}$$

where V_{12} is the element of the scattering matrix containing the scattering potential $V(\mathbf{r}) = K^2[1 - n(\mathbf{r})^2]$. $K = 2\pi/\lambda$ is the wave-vector length in vacuum and $n(\mathbf{r})$ is the refractive index as a function of the coordinates. The averaging $\langle \cdots \rangle$ is performed over the statistical ensemble of all macroscopically nonresolvable roughness profiles.

The essence of the DWBA method consists in splitting the potential V into two parts $V = V^{(0)} + V^{(1)}$, where $V^{(0)}(\mathbf{r})$ represents the undisturbed system (a multilayer with flat interfaces) and $V^{(1)}$ is the disturbance due to the roughness. Within this approximation, the matrix element is[7]

$$V_{12} = V_{12}^{(0)} + V_{12}^{(1)} = \langle \psi_2 | V^{(0)} | \phi_1 \rangle + \langle \psi_2 | V^{(1)} | \psi_1 \rangle, \tag{2}$$

where $|\psi_{1,2}\rangle$ are two independent eigenstates of the undisturbed system and

$$|\phi_1\rangle = \exp(i\mathbf{K}_{\text{in}} \cdot \mathbf{r})$$

is the incident wave corresponding to $|\psi_1\rangle$.

The wave fields $|\psi_m\rangle$ $(m = 1, 2)$ in the undisturbed system are represented by plane waves with amplitudes T_m^j and R_m^j (the amplitudes of the transmitted and reflected waves belonging to the mth eigenstate in the jth layer). The eigenstate $|\psi_2\rangle$ is time inverted.[7] The wave vectors of these waves are denoted $\mathbf{K}_m^j$ and $\mathbf{K}'^j_m$, respectively. The cross section (1) is proportional to the probability of scattering from $|\psi_1\rangle$ into $|\psi_2\rangle$, and the wave vector of the incident and scattered waves are $\mathbf{K}_{\text{in}} = \mathbf{K}_1^1$ and $\mathbf{K}_{\text{out}} = \mathbf{K}_2^1$. These vectors make angles θ_1 (incidence angle) and θ_2 (exit angle) with the sample surface.

The matrix element $V_{12}^{(0)}$ is connected with the complex reflectivity of the undisturbed system[7] and it can be calculated by the standard approach.[8,14] An explicit formula for $V_{12}^{(1)}$ for a general multilayer has been derived in our previous paper.[13] We expressed it in the form of a sum of contributions of particular interfaces

$$V_{12}^{(1)} = \sum_{j=1}^{N} W_j. \tag{3}$$

For the contributions W_j we found the following formula

$$W_j = K^2 (n_j^2 - n_{j+1}^2) \mathbf{E}_2^{j+1\,T} \widehat{\mathbf{F}}^j \mathbf{E}_1^{j+1}. \tag{4}$$

Here

$$\mathbf{E}_m^j = \begin{pmatrix} T_m^j \\ R_m^j \end{pmatrix}$$

is the column vector of the amplitudes of the mth undisturbed state; the superscript T denotes the transposition. The random matrix $\widehat{\mathbf{F}}^j$ contains the roughness profile $U_j(x,y)$

$$\widehat{\mathbf{F}}^j = \begin{pmatrix} F^j(\mathbf{q}_0^{j+1}) & F^j(\mathbf{q}_2^{j+1}) \\ F^j(\mathbf{q}_1^{j+1}) & F^j(\mathbf{q}_3^{j+1}) \end{pmatrix},$$

$$F^j(\mathbf{q}) = \int_S dx dy \int_{z_j}^{z_j + U_j(x,y)} dz \exp(-i\mathbf{q} \cdot \mathbf{r}), \tag{5}$$

where S is the irradiated surface area. The wave vectors $\mathbf{q}^j_{0,\ldots,3}$ are defined as follows:

$$\begin{aligned} \mathbf{q}_0^j &= \mathbf{K}_2^j - \mathbf{K}_1^j, \ \mathbf{q}_1^j = \mathbf{K}'^j_2 - \mathbf{K}_1^j, \\ \mathbf{q}_2^j &= \mathbf{K}_2^j - \mathbf{K}'^j_1, \mathbf{q}_3^j = \mathbf{K}'^j_2 - \mathbf{K}'^j_1. \end{aligned} \tag{6}$$

The intensity of the coherently reflected wave is proportional to the coherent part of $d\sigma$:

$$d\sigma_C = |V_{12}^{(0)} + \langle V_{12}^{(1)} \rangle|^2 / (16\pi^2) d\Omega, \tag{7}$$

where

$$\langle V_{12}^{(1)} \rangle = \sum_{j=1}^{N} \langle W_j \rangle. \tag{8}$$

Thus, within the DWBA approximation, the correlation of roughness profiles of different interfaces does not influence the coherent reflectivity of the multilayer.

The incoherent intensity is proportional to the incoherent part of $d\sigma$:

$$\begin{aligned} d\sigma_I &= \mathrm{Cov}(V_{12}^{(1)}, V_{12}^1) / (16\pi^2) d\Omega \\ &= \sum_{j=1}^{N} \sum_{k=1}^{N} \mathrm{Cov}(W_j, W_k) / (16\pi^2) d\Omega, \end{aligned} \tag{9}$$

where $\mathrm{Cov}(a,b) = \langle ab^* \rangle - \langle a \rangle \langle b \rangle^*$ is the covariance of random quantities a and b. Substituting from (4) into Eq. (9) we get the final formula for the incoherent cross section. This formula contains the covariances,

$$Q_{mn}^{jk} = \mathrm{Cov}[F^j(\mathbf{q}_m^{j+1}), F^k(\mathbf{q}_n^{k+1})];$$

$$m, n = 0, \ldots, 3, \ j, k = 1, \ldots, N,$$

whose explicit forms depend on the defect model chosen.

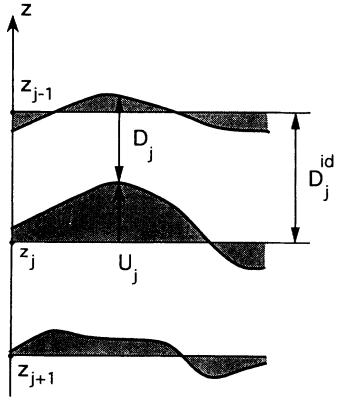

FIG. 1. Sketch of rough interfaces in a multilayer.

III. ROUGHNESS MODELS

We will consider two models of the interface roughness denoted by A and B [see Figs. 2(a),(b)].

Model A: no vertical correlations

Within model A the roughness profile $U_j(x,y)$ is represented by a Gaussian stationary random process with the probability density $N(0,\sigma_j^2)$, where the symbol $N(\mu,\sigma^2)$ denotes the Gaussian probability distribution with the mean value μ and the mean-square deviation σ^2. The correlation properties of this roughness type are expressed by the covariance

$$\mathrm{Cov}[U_j(x,y),U_k(x',y')] \equiv K_{jk}(\rho) = \delta_{j,k}K_j(\rho), \tag{10}$$

where $\rho = \sqrt{(x-x')^2+(y-y')^2}$. The Kronecker delta on the right-hand side of this formula means that the roughness profiles of two different interfaces are not correlated (no vertical correlation). In-plane correlation is described by the in-plane correlation function[7]

$$K_j(\rho) = \sigma_j^2 \exp\left[-\left(\frac{\rho}{\Lambda_j}\right)^{2h_j}\right], \tag{11}$$

containing the in-plane correlation length of the jth interface Λ_j, the rms roughness σ_j, and its fractal dimension $3-h_j$. If $h_j = 1$ the fractal dimension of the interface is 2 (it equals its topological dimension) and the interface has a nonfractal (Gaussian) nature.

Model B: vertical correlations

In model B the actual thickness $D_j(x,y)$ of the jth layer is randomly distributed with probability density $N(D_j^{id},\xi^2)$. Since $U_{j-1} = U_j + D_j - D_j^{id}$, the probability density of U_j is $N(0,\sigma_N^2+(N-j)\xi^2)$, where σ_N is the rms roughness of the substrate surface. The rms roughness of the jth interface is therefore

$$\sigma_j = \sqrt{\sigma_N^2+(N-j)\xi^2} \tag{12}$$

and the interface roughness grows towards the free surface. The covariance of the roughness profiles is

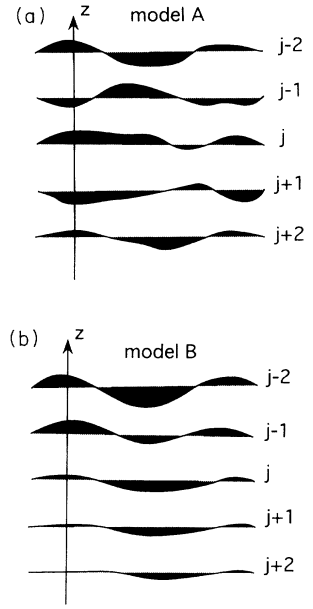

FIG. 2. Models of the interface roughness. (a) Model A: roughness profiles are not correlated, (b) model B: roughness profiles are partially correlated.

$$\begin{aligned}\mathrm{Cov}[U_j(x,y),U_k(x',y')] &\equiv K_{jk}(\rho)\\ &= K_N(\rho) + [N-\max(j,k)]\\ &\quad\times L(\rho).\end{aligned} \tag{13}$$

The roughness profiles of different interfaces are therefore partially correlated (vertical correlation). The first term on the right-hand side of this formula expresses the influence of the substrate roughness; the second one is determined by random fluctuations of the layer thicknesses. The in-plane correlation function $L(\rho)$ of layer thicknesses can be assumed similar to K_j in model A:

$$L(\rho) = \xi^2 \exp\left[-\left(\frac{\rho}{\Lambda}\right)^{2h}\right]. \tag{14}$$

The in-plane correlation length of all interfaces is Λ and their fractal dimension is $3-h$.

Formulas (10) and (13) can be used for calculating the covariances Q_{mn}. After some lengthy calculations we obtained the formula

$$\begin{aligned}Q_{mn}^{jk} = {} & \frac{S}{q_{mz}^{j+1}(q_{nz}^{k+1})^*}\exp[-(\sigma_j q_{mz}^{j+1})^2/2]\exp\{-[\sigma_k(q_{nz}^{k+1})^*]^2/2\}\int_S dxdy\exp[-i(q_x x+q_y y)]\\ & \times\{\exp[q_{mz}^{j+1}(q_{nz}^{k+1})^* K_{jk}(\sqrt{x^2+y^2})]-1\},\ m,n=0,\ldots,3,\ j,k=1,\ldots,N,\end{aligned} \tag{15}$$

where the wave vector transfers $\mathbf{q}_{0,\ldots,3}$ are defined in Eq. (6). From Eq. (11) it follows that in model A $Q_{mn}^{jk} \sim \delta_{j,k}$.

In order to show the role of the vertical roughness correlation, we consider the same rms roughnesses σ_j in both models, i.e., these roughnesses will obey Eq. (12) also in model A. Moreover, within this model we consider the in-plane correlation lengths Λ_j and fractal dimensions $3-h_j$ equal for all interfaces. Then, within both roughness models, the whole roughness structure is characterized by the following parameters: σ_N, the rms roughness of the substrate surface; ξ, the roughness increment in model A or rms deviation of the probability distribution of layer thicknesses in model B; Λ, the in-plane correlation length of all interfaces; and h, the fractal coefficient of all interfaces.

IV. NUMERICAL CALCULATIONS

The above theory has been used for calculations of the intensity reflected from a long-periodic AlAs/GaAs multilayer. The multilayer consists of 20 periods, each period containing one 70-Å GaAs layer and one 150-Å AlAs layer. We assumed the wavelength $\lambda = 1.50$ Å. The total scattered intensity can be expressed as an integral

$$I = I_{\text{in}} \int_{\Omega_{\text{ap}}} \frac{d\sigma}{d\Omega} d\Omega \tag{16}$$

over the entrance aperture angle Ω_{ap} of the detector, where I_{in} is the intensity (photon flux density) of the incident beam. Ω_{ap} can be obtained from the geometrical parameters of the experiment in Table I.

The intensity has been calculated as a function of the wave-vector transfer between the vacuum waves (Fig. 3)

$$\mathbf{q} \equiv \mathbf{q}_0^1 = \mathbf{K}_{\text{out}} - \mathbf{K}_{\text{in}}.$$

This vector depends on the incidence and exit angles $\theta_{1,2}$ as follows:

$$q_x = K(\cos(\theta_2) - \cos(\theta_1)) \tag{17}$$

$$q_z = K(\sin(\theta_2) + \sin(\theta_1)). \tag{18}$$

The conditions $\theta_{1,2} > 0$ determine the accessible part of the reciprocal $q_x q_z$ plane. This part is limited by the Ewald circles $\theta_1 = 0$ and $\theta_2 = 0$; in Fig. 3 these circles are denoted ε_1 and ε_2, respectively. The SXR intensity is distributed along the line $q_x = 0$ in the reciprocal plane.

The coherent part $d\sigma_C$ of $d\sigma$ has been calculated dynamically using the effective complex reflectivities of the interfaces.[8] If the incidence angle is not too large, this method yields the same results as the DWBA.[7] One can then expect that the vertical roughness correlation has a negligible influence on the coherent scattering. The incoherent part $d\sigma_I$ of $d\sigma$ follows from Eqs. (9,15). Similarly to our previous paper,[13] the SXR intensity has been expressed using the sum of $d\sigma_C$ and $d\sigma_I$ weighted by a shape function taking into account the experimental geometry. According to Table I, the detector angular aperture Ω_{ap} is so small that the incoherent component of the SXR intensity is negligible compared with the coherent one. The NSXR intensity has been calculated directly by Eq. (16) using $d\sigma_I$.

Figs. 4(a),(b) show the calculated NSXR intensity distribution in the reciprocal plane using both A and B models. Comparing Figs. 4(a) and 4(b) we can see that

TABLE I. Geometrical parameters of the experiment. The window widths are measured in the θ-2θ plane. The effective width of the detector window is determined by the angular width of the reflection curve of the third crystal (analyzer) and by the sample-analyzer distance.

	Width (μm)	Height (μm)
Input window	50	4000
Effective detector window	40	4000
Sample-detector distance	50 cm	

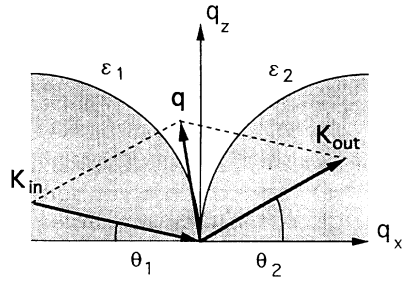

FIG. 3. Scheme of the wave-vector transfer in the reciprocal plane. The shaded areas are inaccessible by nonspecular scattering.

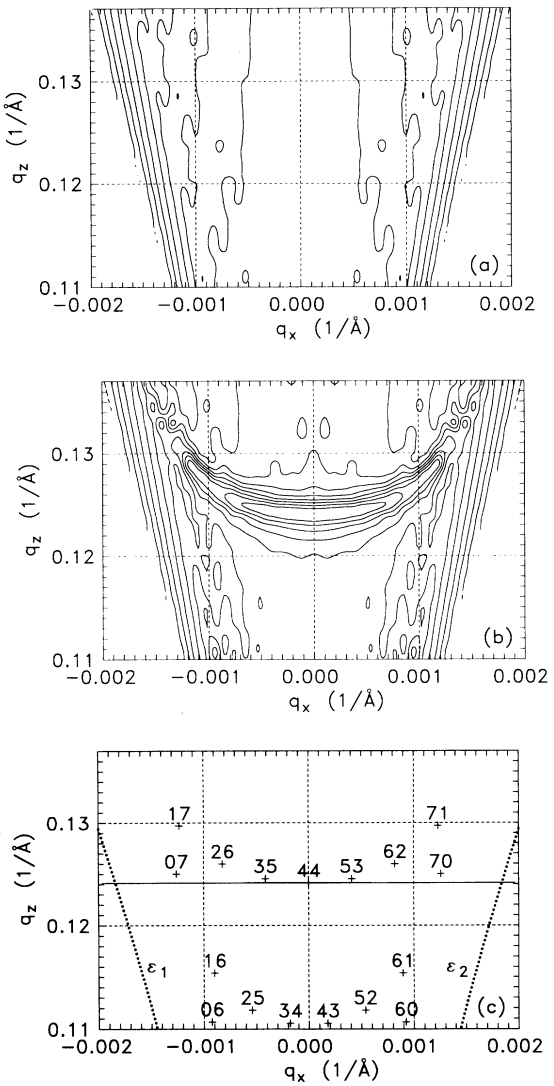

FIG. 4. Nonspecular intensity distribution in the reciprocal plane calculated for a periodical AlAs/GaAs multilayer using (a) model A and (b) model B. The roughness parameters are $\sigma_N = 8.6$ Å, $\xi = 1.6$ Å, $\Lambda = 2000$ Å, and h=1. The neighboring contours represent the intensity ratio $10^{0.2}$. (c) shows the positions of the R_1R_2 BL peaks following from Eq. (21) and the Ewald circles $\varepsilon_{1,2}$ denoted by the dotted lines. The continuous line is the trajectory of the ω scan going through the 44 peak.

without the vertical roughness correlation (model A) the NSXR intensity is distributed into a broad vertical zone along the q_z axis. The width of this zone in the q_x direction is proportional to $1/\Lambda$. With the vertical correlation (model B) the NSXR distribution is quite different. The intensity is concentrated in stripes, and far from the TER region these stripes are straight and parallel with q_x. Near the TER region they are curved so that they approach the Ewald circles $\varepsilon_{1,2}$. Similarly to model A, the size of the stripe in the q_x direction is proportional to $1/\Lambda$. In the q_z direction, however, its size depends on the rms roughness and on the multilayer thickness.

The intensity distribution can be measured along certain lines in the reciprocal plane. In the so-called ω scan it is measured along the line $\theta_1 + \theta_2 = 2\theta$ =const. This line (scan trajectory) approaches the line q_z =const, if the angles $\theta_{1,2}$ are sufficiently small [see Fig. 4(c)]. Figures 5(a),(b) show these scans calculated in models A and B along the trajectories going through the third and fourth Bragg peaks in the coherent reflectivity as well as between them.

In the 2θ scan the scattered intensity is measured along the trajectory θ_1 =const. Fig. 6(a) shows this scan calculated for θ_1 corresponding to the fourth Bragg peak of the coherent reflectivity.

The SXR intensity is measured along the line $q_x = 0$ in the ω-2θ scan. In the case of larger angular detector aperture Ω_{ap} (using a detector slit instead of the analyzer crystal, for instance) the diffuse contribution to the SXR intensity cannot be neglected. Figure 6(b) demonstrates the diffuse contribution to the ω-2θ scan calculated for both roughness models.

In all scan types, several intensity maxima can be observed. The concentration of the NSXR intensity into the stripes is the cause of the resonant diffuse scattering peaks, dynamical scattering processes giving rise to the Yoneda peaks and the Bragg-like peaks. These peaks will be discussed in Sec. VI.

V. EXPERIMENTS

SXR and NSXR were measured from an AlAs/GaAs multilayer with 20 periods grown by molecular-beam epitaxy (MBE) on a [001]-oriented GaAs substrate. The x-ray experiments were performed with the triple crystal diffractometer of the D23 beamline at LURE, University Paris-Sud, using synchrotron radiation. The wavelength 1.5 Å was selected by a Si (111) double monochromator, and Ge (111) was applied as an analyzer crystal. The

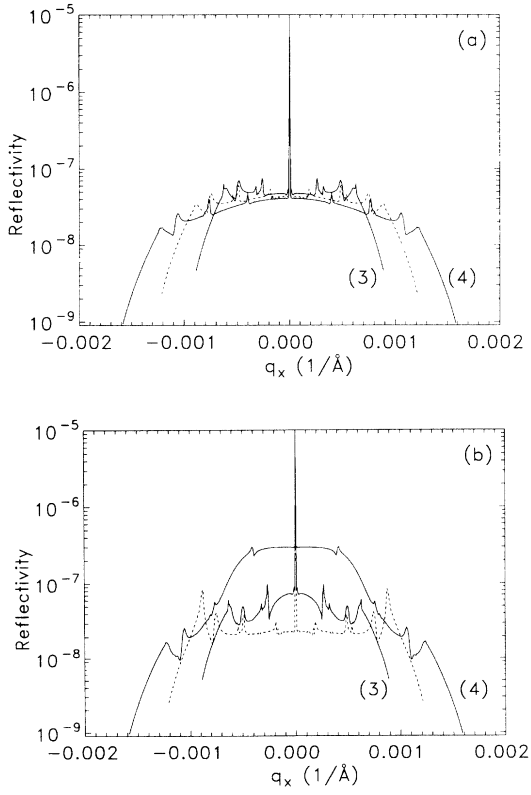

FIG. 5. ω scans calculated for roughness parameters identical with those in Fig. 4. The scan trajectories were assumed going through the third Bragg peak [line (3)] and the fourth Bragg peak [line (4)]. The dashed line shows the ω scan with trajectory between those Bragg peaks. The roughness models A (a) and B (b) were considered.

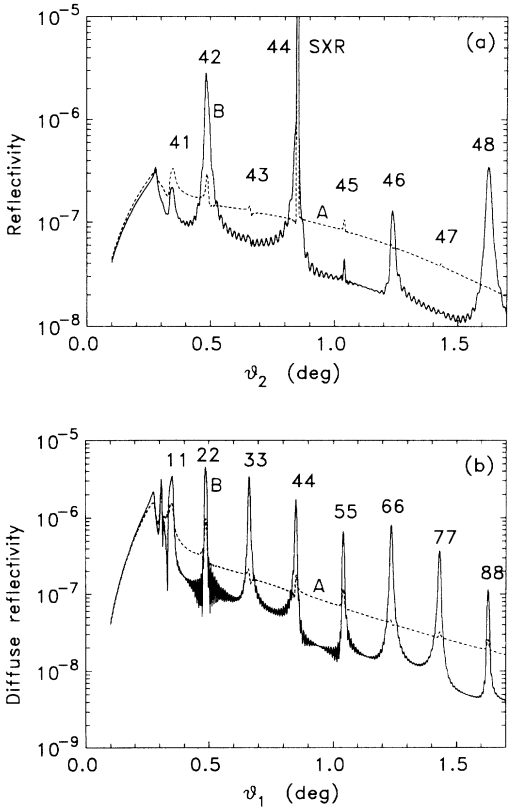

FIG. 6. 2θ scans (a) and the diffuse component of the ω-2θ scans (b) calculated for the same roughness parameters as in Fig. 4. Roughness model A is shown with dashed lines and model B with continuous lines. The 2θ scans in (a) are calculated for the incidence angle θ_1 corresponding to the fourth Bragg peak in the coherent reflectivity curve. The numbers denote the indices p_1p_2 of the R_1R_2 BL peaks and the specular peak in (a) is denoted by SXR.

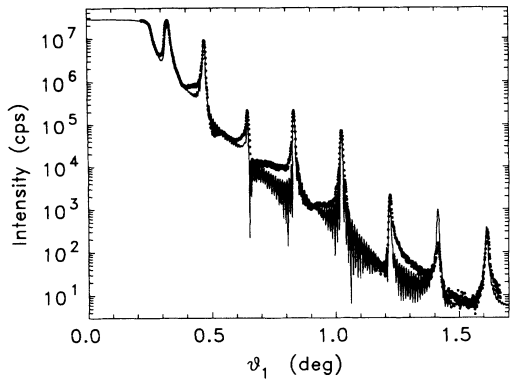

FIG. 7. ω-2θ scan measured (points) on an AlAs/GaAs multilayer. The line represents the best fit from the theory.

geometrical characteristics of the experimental setup are in Table I.

We measured the SXR intensity in the ω-2θ scan and the NSXR in the ω scans. Figure 7 shows the measured SXR intensity. The experimental curve has been fitted with the theoretical one calculated by means of the effective reflectivities (we neglected the incoherent contribution to the measured SXR intensity). From the fit we obtained the roughness values $\sigma_N = (8.6 \pm 0.7)$ Å, $\xi = (1.6 \pm 0.2)$ Å, and the layer thicknesses $T_{\mathrm{GaAs}} = (68 \pm 1)$ Å and $T_{\mathrm{AlAs}} = (146 \pm 2)$ Å. The theoretical curve fits the experimental one quite well except for the seventh Bragg peak.

The measured ω scans across the third and fourth Bragg peaks are in Fig. 8. From the fit with the theory (roughness model B) we estimated the in-plane correlation length $\Lambda = (2000 \pm 500)$ Å (from both scans), taking the rms roughnesses from the fit of the ω-2θ scan.

VI. DISCUSSION

Three types of maxima of the NSXR distribution in the reciprocal plane can be established: (1) resonant diffuse scattering (RDS) peaks, (2) the Yoneda wings, and (3) the Bragg-like (BL) peaks.

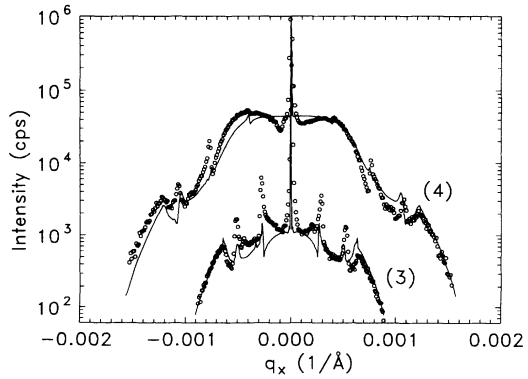

FIG. 8. ω scans (points) measured along trajectories going through the third [line (3)] and the fourth Bragg peaks [line (4)]. Line (4) is shifted upwards by a factor of 10. The lines are the best theoretical fits.

Resonant diffuse scattering

If the roughness profiles of different interfaces are partially correlated, the distribution of the diffusely scattered intensity exhibits maxima in reciprocal space (resonant diffuse scattering). The intensity is concentrated into stripes going through the lattice points of the one-dimensional reciprocal lattice of the multilayer. The distance of these stripes in the q_z direction is therefore $2\pi/D$, where D is the multilayer period. If x-ray refraction can be neglected, these maxima are straight and parallel with the layer interfaces.

The concentration of the NSXR intensity in sheets parallel with the layers in the correlated case has been postulated previously,[3] without taking into account the bending of the sheets due to x-ray refraction. In Ref. 6 the RDS effect has been documented by calculating the integral value of the NSXR intensity as a function of the incidence angle. A similar distribution of the diffusely scattered intensity can be established[15] by x-ray diffraction from rough single-crystal periodic multilayers. If the roughness is vertically correlated, the diffusely scattered waves accompanying the diffracted beams are concentrated in straight sheets parallel with the layers going through the satellite reciprocal-lattice points.

If the line scan trajectory intersects the RDS maxima in reciprocal space, RDS peaks occur in the intensity distribution curve. The shape of the peaks depends on the scan trajectory. The trajectory of a ω scan is nearly parallel with the stripes (the stripes are only slightly curved due to x-ray refraction), and, therefore, the ω scan contains only one RDS maximum having the form of a broad hump near the specular peak. This hump disappears in the ω scans between the stripes [Fig. 5(b)] and no RDS maximum can be established within model A [no vertical roughness correlation, Fig. 5(a)].

In a 2θ scan a number of these peaks can be found [Fig. 6(a)]. Comparing the radius of the 2θ scan trajectory (the Ewald sphere) with the distance of the RDS stripes we find that the angular distance of the RDS peaks in this scan is about

$$\Delta\theta_2^{\mathrm{RDS}} \approx \lambda/D.$$

The incoherent part of the SXR intensity measured in the ω-2θ scan exhibits RDS maxima, too [Fig. 6(b)]. Simple geometrical considerations show that the angular distance of these peaks is

$$\Delta\theta_1^{\mathrm{RDS}} \approx \lambda/(2D).$$

The RDS effect can be described by means of the Born approximation as well. In this approach the states $|\psi_{1,2}\rangle$ are two independent eigenstates of the vacuum wave equation

$$|\psi_1\rangle = |\phi_1\rangle = \exp(i\mathbf{K}_{\mathrm{in}} \cdot \mathbf{r}); \; |\psi_2\rangle = \exp(i\mathbf{K}_{\mathrm{out}} \cdot \mathbf{r}). \quad (19)$$

Figure 9(a) shows the distribution of the NSXR inten-

sity calculated with the vertical correlation (model B) in the BA. The stripes of the NSXR maxima create a one-dimensional reciprocal lattice parallel with q_z with the lattice parameter $2\pi/D$. X-ray refraction is neglected so that the stripes are straight.

The BA approach can be improved by replacing the vacuum states by the plane waves propagating in an averaged medium with the mean refraction index n:

$$|\psi_1\rangle = \exp(i\mathbf{K}_1^{\mathrm{av}} \cdot \mathbf{r}); \ |\psi_2\rangle = \exp(i\mathbf{K}_2^{\mathrm{av}} \cdot \mathbf{r}). \qquad (20)$$

Then, x-ray refraction and reflection (TER) are taken into account giving the NSXR distribution in Fig. 9(b). The stripes are curved in the same way as those from the exact calculation [Fig. 4(b)]; the other peaks (the Yoneda peaks and Bragg-like peaks) are not present.

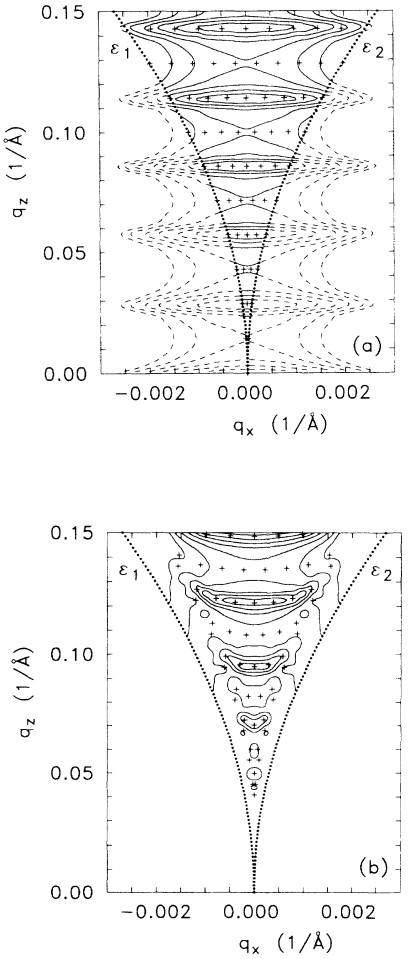

FIG. 9. Nonspecular intensity distribution in the reciprocal plane calculated within the first Born approximation without (a) and with (b) x-ray refraction. Crosses denote the positions of the R_1R_2 BL peaks. The dotted lines represent the Ewald circles $\varepsilon_{1,2}$. The NSXR intensity in the inaccessible regions of (a) is denoted by dashed lines. The roughness parameters are the same as in Fig. 4, and roughness model B is assumed.

The Yoneda peaks

Unlike the RDS peaks, the Yoneda and Bragg-like peaks are caused by multiple scattering processes so that they have purely dynamical nature. The Yoneda peaks occur if the angles of incidence θ_1 and/or exit θ_2 equal the critical angle θ_c of TER. Those peaks follow from DWBA calculations and, in addition, they can be included in BA formulas by multiplying $|\psi_{1,2}\rangle$ in Eq. (20) by the complex transmittivities of the averaged medium surface.

The Bragg-like peaks

The positions of the Bragg-like (BL) peaks can be understood using the concept of *Umweganregung*.[16,17] In our sense, the *Umweganregung* means the excitation of a scattering process (leading to the Bragg-like peaks) by another scattering process (RDS scattering). Four diffuse scattering processes and consequently 16 terms of covariances Q_{mn} have to be taken into account for calculating the resulting intensity. The scattering processes can be interpreted as a primary scattering with the wave vector transfer $\mathbf{q}_0$ (scattering of the transmitted wave into the transmitted wave again with the amplitude T_1T_2) and three processes of *Umweganregung* with the wave-vector transfers $\mathbf{q}_{1,2,3}$ (the processes T_1R_2, T_2R_1, and R_1R_2, respectively).

The last three processes occur only if the reflected waves $R_{1,2}$ in the states $|\psi_{1,2}\rangle$ are present, i.e., if the angles θ_1 or θ_2 obey the modified Bragg equation

$$2D\sqrt{n^2 - \cos^2(\theta_m^{\mathrm{BL}})} = p_m\lambda; \ m = 1, 2. \qquad (21)$$

Here n is the mean refraction index, D is the multilayer period, and $p_{1,2}$ are integers denoting the orders of the BL peaks. The T_1R_2 and R_1T_2 BL peaks are stretched along the Ewald spheres $\theta_2 = \theta_2^{\mathrm{BL}}$ =const and $\theta_1 = \theta_1^{\mathrm{BL}}$ =const, respectively (Fig. 10). The process R_1R_2

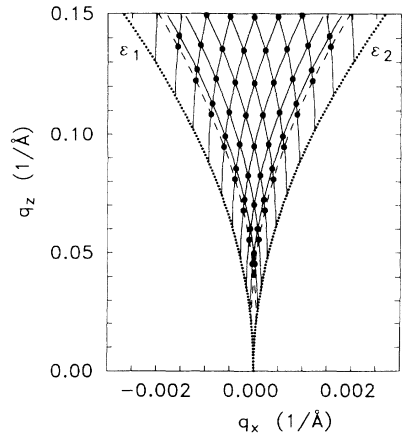

FIG. 10. Distribution of the BL peaks in the reciprocal plane. Dotted lines are the Ewald circles $\varepsilon_{1,2}$ defining the inaccessible regions, dashed lines are the positions of the Yoneda peaks, and continuous lines express the positions of BL peaks of types R_1T_2 and T_1R_2. The isolated R_1R_2 BL peaks are denoted by black dots.

yields sharp BL peaks in points $\theta_1 = \theta_1^{\mathrm{BL}} \cap \theta_2 = \theta_2^{\mathrm{BL}}$. These BL peaks are depicted in Figs. 4(c), 9(a), 9(b), and 10.

The positions of BL peaks do not depend on the roughness properties; they are only influenced by the undisturbed multilayer structure, mainly by the multilayer period. The form of the BL peaks in the line scans depends on the mutual position of the scan trajectory and the BL maxima in reciprocal space. The trajectories of the ω scans can intersect the sharp R_1R_2 maxima only incidentally and the sharp resonant peaks in these scans are mainly caused by the processes T_1R_2 and R_1T_2.

If we perform a 2θ scan with the incidence angle θ_1 obeying the Bragg formula (21) the scan trajectory goes along the maximum of the R_1T_2 process and it intersects the isolated maxima R_1R_2 in reciprocal space (Fig. 10). Therefore, the resonant peaks observed in this scan [Fig. 6(a)] are caused mainly by the R_1R_2 scattering. In Fig. 6(a), the indices $p_{1,2}$ of those peaks are depicted. The angular distance of those peaks in a 2θ scan follows from the Bragg law (21)

$$\Delta\theta_2^{BL} \approx \lambda/(2D),$$

so that $\Delta\theta_2^{RDS} \approx 2\Delta\theta_2^{BL}$. This is demonstrated in Fig. 6(a), where the curve A (no vertical correlation) contains only BL peaks and curve B (with the vertical correlation) contains both BL and RDS maxima. Every second BL peak is enhanced due to the RDS effect. It is worth mentioning that the forms of the two peak types are different. The RDS peaks are nearly symmetrical, whereas the BL peaks are S-shaped. Similar behavior can be found in Figs. 9(a),(b). The RDS stripes lie along the rows of the R_1R_2 BL peaks with the indices $p_1 + p_2 = 0, 2, 4, \ldots$, while those with $p_1 + p_2 = 1, 3, 5, \ldots$ are between the RDS stripes.

From the NSXR distributions in Figs. 9(a),(b) it follows that in a ω-2θ scan, the RDS and BL maxima of the diffuse intensity coincide and their separation is equal. The trajectory $q_x = 0$ of this scan goes through the R_1R_2 BL peaks with the indices 11, 22, 33,... and these peaks lie in the RDS stripes. This is demonstrated in Fig. 6(b), where the RDS peaks in curve B coincide with BL peaks in curve A.

From the DWBA theory it follows that the coherently reflected intensity does not depend on the degree of vertical roughness correlation. This finding has been supported elsewhere[6] by another method.

In our calculations we have restricted ourselves to the case $h = 1$, i.e., we have assumed the nonfractal (Gaussian) nature of the interfaces. A detailed statistical description of a rough interface of a multilayer has demonstrated[18] that in MBE-grown multilayers $h = 0.5$ holds. In our previous paper[13] we have shown that in the region $0.5 \leq h < 1$ the NSXR intensity depends only slightly on h. The assumption $h = 1$ allowed us to use a more efficient numerical procedure for calculating NSXR.

From the coincidence of the measured and theoretical NSXR distributions it follows that the actual roughness structure of the multilayer corresponds rather to model B (with vertical correlation) than to model A. We believe the discrepancies in the resonant peak shapes are not caused by the roughness but, most likely, by the DWBA approximation itself.

VII. CONCLUSIONS

The distorted-wave approach has been used for calculating the intensity of the waves reflected nonspecularly from a rough multilayer. It has been demonstrated theoretically that the correlation of the roughness profiles of different interfaces plays a crucial role in the distribution of nonspecularly scattered intensity in the reciprocal plane. If the interface roughness profiles are partially correlated, the diffusely scattered intensity is concentrated in stripes of the reciprocal plane going through the resonant maxima. This behavior has been proved experimentally and a good fit has been found of the experimental nonspecular intensity distribution with the theory.

ACKNOWLEDGMENTS

The authors would like to thank F. Morier-Genoud and D. Martin from the Institut de Micro- et Optoélectronique, Lausanne (Switzerland) for the sample preparation and H. Fischer and M. Bessiere from LURE, Université Paris–Sud, Orsay (France) for providing the experimental equipment and technical assistance. It is a pleasure to acknowledge M. Gailhanou (Institut de Micro- et Optoélectronique, Lausanne, Switzerland) for assistance with the measurements, and fruitful discussions with J. Kuběna, University Brno (Czech Republic).

[1] D.G. Stearns, J. Appl. Phys. **65**, 491 (1989).
[2] D.G. Stearns, J. Appl. Phys. **71**, 4286 (1992).
[3] D.E. Savage, J. Kleiner, N. Schimke, Y.-H. Phang, T. Jankowski, J. Jacobs, R. Kariotis, and M.G. Lagally, J. Appl. Phys. **69**, 1411 (1991).
[4] D.E. Savage, N. Schimke, Y.-H. Phang, and M.G. Lagally, J. Appl. Phys. **71**, 3283 (1992).
[5] Y.-H. Phang, R. Kariotis, D.E. Savage, and M.G. Lagally, J. Appl. Phys. **72**, 4627 (1992).
[6] A.P. Payne and B.M. Clemens, Phys. Rev. B **47**, 2289 (1993).
[7] S.K. Sinha, E.B. Sirota, S. Garoff, and H.B. Stanley, Phys. Rev. B **38**, 2297 (1988).
[8] L. Névot and P. Croce, Rev. Phys. Appl. **15**, 761 (1980).
[9] D.K.G. de Boer, Phys. Rev. B **44**, 498 (1991), and the citations therein.
[10] D. Bahr, W. Press, R. Jebasinski, and S. Mantl, Phys. Rev. B **47**, 4385 (1993).

[11]J.B. Kortright, J. Appl. Phys. **70**, 3620 (1991).
[12]X. Jiang, T.H. Metzger, and J. Peisl, Appl. Phys. Lett. **61**, 904 (1992).
[13]V. Holý, J. Kuběna, I. Ohlídal, K. Lischka, and W. Plotz, Phys. Rev. B **47**, 15 896 (1993).
[14]G. Parrat, Phys. Rev. **95**, 359 (1964).
[15]V. Holý, Appl. Phys. A (to be published).
[16]T. Baumbach, V. Holý, U. Pietsch, and M. Gailhanou, Physica B (to be published).
[17]M. Renninger, Z. Kristallogr. **106**, 141 (1937).
[18]V. Holý, J. Kuběna, and I. Ohlídal, Superlatt. Microstruct. **12**, 25 (1992).

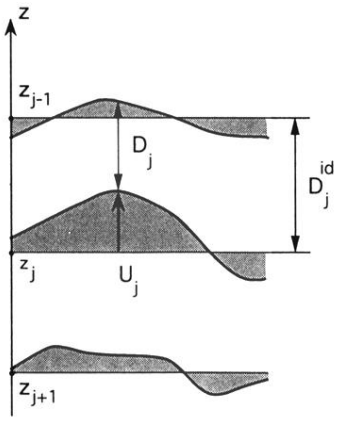

FIG. 1. Sketch of rough interfaces in a multilayer.

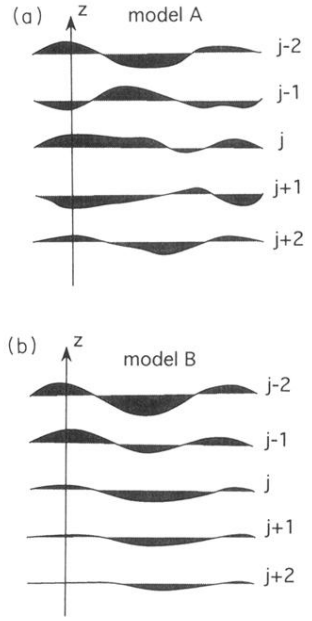

FIG. 2. Models of the interface roughness. (a) Model A: roughness profiles are not correlated, (b) model B: roughness profiles are partially correlated.

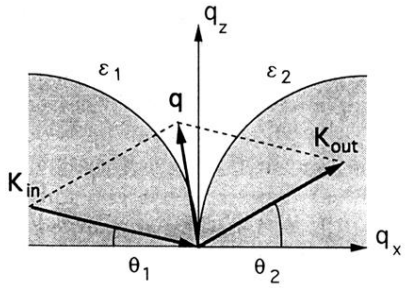

FIG. 3. Scheme of the wave-vector transfer in the reciprocal plane. The shaded areas are inaccessible by nonspecular scattering.